remote sensing

MDPI

Article

A Framework Analyzing Climate Change, Air Quality and Greenery to Unveil Environmental Stress Risk Hotspots

Priyanka Rao, Patrizia Tassinari and Daniele Torreggiani *

Department of Agricultural and Food Sciences, University of Bologna, 40126 Bologna, Italy; priyanka.rao2@unibo.it (P.R.); patrizia.tassinari@unibo.it (P.T.)
* Correspondence: daniele.torreggiani@unibo.it

Abstract: Rapid urbanization has resulted in increased environmental challenges, compounding worries about deteriorating air quality and rising temperatures. As cities become hubs of human activity, understanding the complex interplay of numerous environmental elements is critical for developing effective mitigation solutions. Recognizing this urgency, a framework to highlight the hotspots with critical environmental issues emerges as a comprehensive approach that incorporates key criteria such as the surface urban heat island intensity (SUHII), heat index (HI) and air quality index (AQI) to assess and address the complex web of environmental stressors that grip urban landscapes. Employing the multicriteria decision analysis approach, the proposed framework, named the environmental risk hotspot mapping framework (ERHMF), innovatively applies the analytic hierarchy process at a sub-criteria level, considering long-term heat island trends with recent fluctuations in the HI and AQI. Climate change impact has been symbolized through rising temperatures, as reflected by surface urban heat island intensity trends over two decades. The robustness and correctness of the weights have been assessed by computing the consistency ratio, which came out as 0.046, 0.065 and 0.044 for the sub-criteria of the SUHII, AQI and HI, respectively. Furthermore, the framework delves into the nexus between environmental stressors and vegetation cover, elucidating the role of green spaces in mitigating urban environmental risks. Augmented by spatial and demographic data, the ERHMF adeptly discerns high-risk areas where environmental stress converges with urban development, vulnerable population concentrations and critical vegetation status, thereby facilitating targeted risk management interventions. The framework's effectiveness has been demonstrated in a regional case study in Italy, underscoring its ability to pinpoint risk hotspots and inform specific policy interventions. The quantitative study undertaken at the sub-administrative level revealed that approximately 6,000,000 m^2 of land in Bologna are classified as being under high to extremely high environmental stress, with over 4,000,000 m^2 lying only within the extremely high stress group (90–100). Similarly, 1,000,000 m^2 of land in Piacenza and Modena have high levels of environmental stress (80–90). In conclusion, the ERHMF presents a holistic methodology for delineating high-risk urban hotspots, providing essential insights for policymakers, urban planners and stakeholders, with the potential to enhance overall urban resilience and foster sustainable development efforts.

Keywords: remote sensing; urban heat island; environmental stress; risk framework; hotspot; multicriteria analysis

Citation: Rao, P.; Tassinari, P.; Torreggiani, D. A Framework Analyzing Climate Change, Air Quality and Greenery to Unveil Environmental Stress Risk Hotspots. *Remote Sens.* **2024**, *16*, 2420. https://doi.org/10.3390/rs16132420

Academic Editor: Carmine Serio

Received: 7 May 2024
Revised: 20 June 2024
Accepted: 28 June 2024
Published: 1 July 2024

1. Introduction

It has been projected that around two-thirds of the global population will reside in urban areas by 2050 (source: https://www.un.org/development/desa/en/news/population/2018-revision-of-world-urbanization-prospects.html (accessed on 15 November 2023)). Moreover, Europe is expected to have an urbanization rate of approximately 84% by the same year. The migration to urban centers contributes to agricultural land abandonment, which is expected to reach 4.2 million hectares by 2030 [1,2]. Based on an official report [3], the expansion of built-up areas is expected in most EU countries by 2030, with Italy being

on top in terms of an absolute increase (an additional 144 thousand hectares). In this line, several studies have been performed analyzing the alterations in the landscape settings. For example, ref. [4] have developed a methodology for the classification and analysis of a unique urban–rural–natural gradient, i.e., a combination of the main landscape change drivers' specific interactive environmental gradients and natural components, based on CORINE land cover. Another study [5] has resulted in a framework creating similar networks in different landscapes based on multiple drivers, leading to landscape adaptation plans for climate change. Machine learning for a spatiotemporal analysis of the surface temperature and land use indices to highlight inter-urban interactions between temperature and land use parameters were utilized [6].

The rapid growth of the urban population has significantly altered urban land cover and led to a substantial rise in energy consumption, leading to several environmental issues. Moreover, extreme weather conditions related to temperature and humidity, along with deteriorating air quality, are exerting a growing negative health impact on the global population, typically in urban areas. Notably, surface thermal stress (surface urban heat island (SUHI)), atmospheric thermal stress (heat index (HI)) and air pollution (air quality index (AQI)) effects stand out as typical environmental concerns [7,8]. Higher temperatures intensify the urban heat island (UHI) effect, which is typically referred to as increased urban area temperature compared to rural or suburban surroundings.

Extreme heat events intensify the UHI effect, under the influence of urban surface characteristics like limited vegetation cover, anthropogenic heat emission and alterations in air flow patterns due to buildings and asphalt streets [9]. UHIs have detrimental effects on human health and the environment, in terms of the increased demand of energy-intensive cooling systems in buildings [10], leading to high greenhouse gas emissions and degraded air quality [11–13]. This creates a feedback loop and exacerbates the negative impacts of global warming. Therefore, increased temperature in collaboration with major air pollutants leads to increased physiological strain and vulnerability, exposing people to higher risks, certainly urban residents [7,14–16]. It has been demonstrated that the implementation of sustainable urban planning practices and smart city design, comprising urban green spaces, green roofs and cool pavements, holds significant potential in mitigating UHI effects and reducing air pollution [17]. Moreover, it has been proposed that to deal with environmental stress, green infrastructure should be rooted and designed based on the specific geographical context considering multiple parameters [18]. Specifically, these measures have shown promising results in decreasing the level of ozone, nitrogen dioxide and particulate matter (PM_{10}) in urban environments [9]. In addition, several attempts have been made to analyze and compare green spaces and their impacts on the environment and human health. For example, ref. [19] compare several green space types and their relation with mental health. Subsequently, ref. [20] propose the demand and supply-based model for identifying the locations to implant urban trees for the mitigation of air pollution. Further, the efficacy of the worldview-3 data for carbon stock mapping has been tested based on the available Light Detection and Ranging (LIDAR) datasets in a specific urban area to find a more affordable and easy alternative to map the carbon stocks in developing countries for the efficient green management planning [21]. However, appropriate identification of the potential spots to implement the climatic stress mitigation measures, along with considering the temporal impacts, is still lacking in the ongoing urban research [22]. Therefore, a detailed framework based on multiple criteria covering major thermal and air stress-based issues could be an asset in planning sustainable and healthy cities, because if not dealt with appropriately, these stressors together can lead to a highly unpleasant living environment with increased health issues, including cardiovascular and respiratory issues [23].

Recently, there has been a growing research focus on addressing the combined effects of thermal stress and air pollution. Comprehensive reviews spanning the last three decades highlight the importance of studying the synergistic effects of the UHI, HI and air pollution as an integrated research direction [10]. This approach recognizes the re-

lationship between thermal stress and air pollution, highlighting the need for a holistic understanding to effectively mitigate their adverse consequences [24]. Moreover, in the realm of intensity index calibration methodologies, multicriteria decision analysis (MCDA) approaches have demonstrated notable effectiveness in incorporating both qualitative and quantitative data for different analyses in varied domains [25]. Among these approaches, the analytic hierarchy process (AHP) is widely used for understanding hazard and risk phenomena [26]. Recent MCDA-based studies have used the AHP, interval-fuzzy AHP (FAHP) and analytic network process with geographical information system (GIS) together to study risk assessment [27]; highlighted the importance of GIS and MCDA methods for flood risk models [28]; and compared the FAHP and G-DEMATEL-AHP approaches for identifying the critical risk areas for floods [29]. Maximum MCDA models have focused on single risk categories, like floods; therefore, considering the increasing heat stress and air pollution, it is necessary to design an appropriate risk assessment framework for the urban environment with adequate optimizations. The optimization procedures facilitate the calibration of multiple indices and variables associated with thermal and environmental factors, enabling their integration for risk assessment. Fine-tuning variables and indices based on time-series observations helps enhance the effectiveness of MCDA methods [30].

The existing literature has typically investigated these parameters either individually or by comparison, maintaining a single parameter under the spotlight, for example, either the UHI or meteorological variables or anthropogenic heat or urban morphology, etc. [31–34]. In addition, a more detailed understanding of the role of existing green spaces in the urban environment by analyzing its relation with environmental stress parameters is also an important aspect to be addressed [35]. Hence, this framework design has filled this research gap by evaluating spatiotemporal information about the surface and air thermal stress based on different indices and variables, along with analyzing the air quality components based on their AQI concentrations, together in a single frame. These indicators have been also individually analyzed on a spatiotemporal scale to study their impact. Hence, this study is aligned toward designing a detailed and integrated risk evaluation framework to identify and highlight areas requiring immediate attention for mitigating harmful consequences of the increasing environmental stress. This study introduces and assesses an MCDA-based environmental risk hotspot mapping framework (ERHMF). It aims to identify specific areas, defined as hotspots, where thermal and air quality stress, and vegetation-based criticality, intersect with exposure and vulnerability, leading to higher risk considering climate change and urbanization. To evaluate the environmental stress, multiple risk criteria have been analyzed during the summer months and integrated through the AHP. These criteria include the less explored indices, derived based on environmental stress criteria. The framework's effectiveness is tested and evaluated in the Emilia-Romagna (ER) region of Italy. It integrates environmental risk criteria, temporal aspects, demographics data and vegetation status to analyze them both spatially and quantitatively to prioritize environmental interventions effectively. Our contributions to this study are as follows:

1. We design an environmental stress framework to incorporate multiple environmental stress criteria by computing rarely explored indices for each criterion and analyzing their temporal trend;
2. We compute the preference weights using a decision-making framework that involves breaking down a complex decision into a hierarchical structure of criteria;
3. We establish a correlation between environmental stress and vegetation and calculate the hotspots of environmental risk by considering factors such as stress severity, exposure, vulnerability and the criticality of vegetation status.

The remainder of this paper is organized as follows. Section 2.2 formally defines the study area and materials. Section 3 presents the applied methods. Section 4 describes the results and discussions. Finally, Section 5 draws the concluding remarks of our paper.

2. Study Area and Dataset Used

2.1. Study Area

The ER region, located in northern Italy, encompasses the former territories of Emilia and Romagna, where the Po Plain and northern Apennines converge. It is one of Italy's 20 administrative regions, ranking sixth in terms of area. According to the National Institute of Statistics (2018), with nine provinces spread over 22,446 km^2, ER covers a significant percentage of the country. Its landscape consists of plains (48%), mountains (25%) and hilly areas (27%). The region is home to approximately 4.4 million people, with three-fourths residing in the plains. Bologna, Parma, Modena, Reggio Emilia, Ravenna, Rimini, Ferrara, Forli and Piacenza are the nine major cities, each having a population exceeding 100,000 and listed among the top fifty most populous cities in the country. Figure 1 illustrates the geographical location and spatial arrangement of the province in the ER region, along with the weather station locations used in this study.

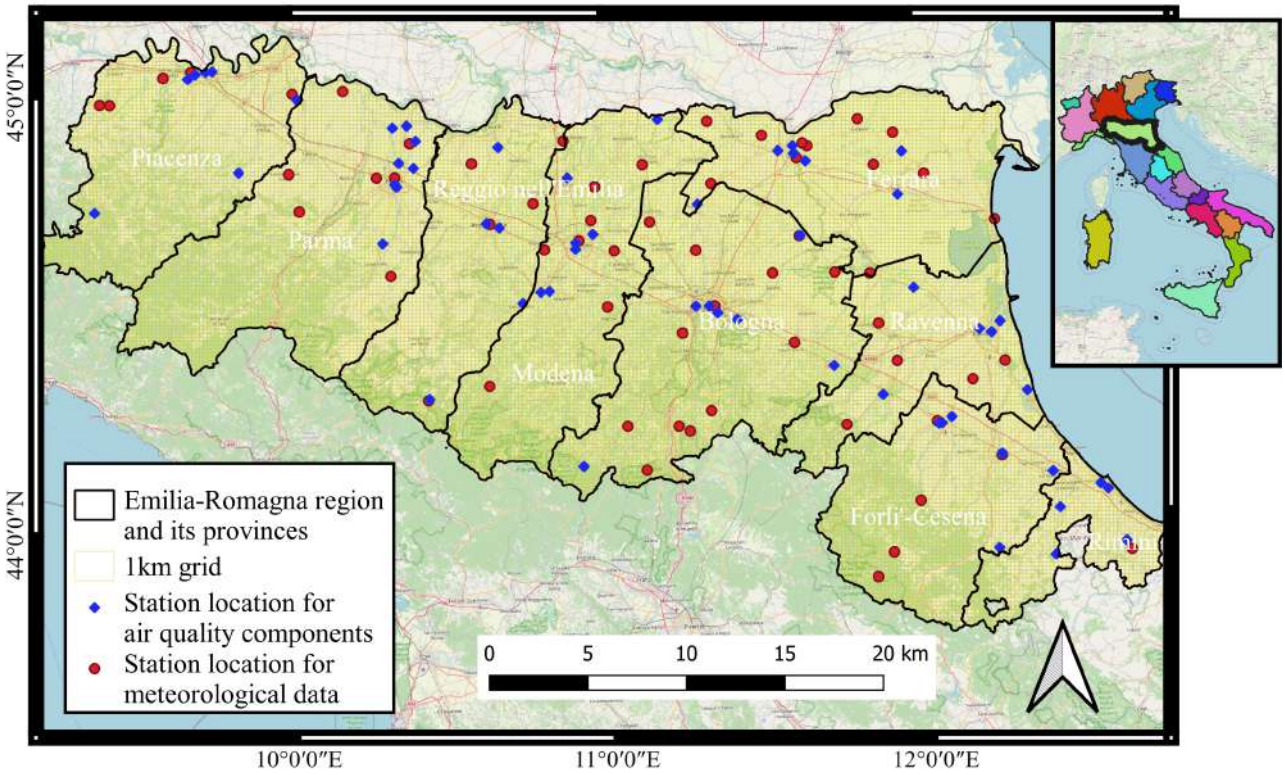

Figure 1. Study area map highlighting Emilia-Romagna region with its provinces' boundaries. In addition, the colored dots represent the location of stations for air quality (blue) and meteorological (red) data for estimation of environmental stress magnitude; key map on top right corner shows regional distribution of Italy.

The landscape of the region has varied relief properties, influencing the distribution of vegetation types. The mountains and hilly regions are majorly dominated by coniferous and broad-leaved forests, whereas the plains and lowlands are rich with grasslands and croplands. The coastal areas are characterized by Mediterranean pine and cypress. The climate observed in Po Plain and the hilly areas is subcontinental; however, it has a cool temperate type in the mountainous areas. According to the Koppen–Geiger climate classification, a temperate climate type with completely hot and humid summers (Cfa) is predominantly observed over the northeast side of the ER region, while fully humid and warm summers (Cfb) are observed in the southwest part of the region [36,37]. As the climate type is strongly influenced by the physical characteristics of the region, the northern Apennines witness over 2000 mm of precipitation, whereas less than 800 mm is observed in the eastern Po Plain. During the summer, the ER region experiences the

highest temperatures and lowest rainfall in Northern Italy. Thunderstorms occur occasionally but less frequently compared to the northern part of the Po Valley. The average summer temperatures range from 24 to 24.5 °C along the coast (Cervia and Rimini) and reach nearly 26 °C in the central area (Reggio-Emilia, Modena and Ferrara). The hottest temperatures are typically observed in the central-western region, particularly around Ferrara and the lower plain of the Modena and Bologna provinces, exceeding up to 40 °C (source: hhttps://www.climatestotravel.com/climate/italy/emilia-romagna (accessed on 15 November 2023)).

2.2. Datasets Used

This study utilizes satellite datasets obtained through the Google Earth Engine (GEE), a cloud computing platform. The GEE enables users to perform various geospatial analyses, like the assessment, visualization, analysis and download of a wide range of global satellite data [38–40]. It is a widely recognized and important tool in the geospatial field due to its user-friendly application programming interface (API), facilitating easy analysis of large and freely available satellite datasets [38]. The datasets acquired from the GEE are ensured with the permissible cloud clover of satellite images, i.e., <20 (%).

This study examines environmental variables like the SUHI intensity (SUHII), air quality and HI, derived from weather parameters acquired from AQICN (source: https://aqicn.org/data-platform/ (accessed on 15 November 2023)) and Dexter (source: https://simc.arpae.it/dext3r/ (accessed on 15 November 2023)). As the SUHII and HI refer to surface and atmospheric thermal stress, respectively, the long-term SUHII trend analysis is a holistic approach to examine the surface thermal properties and land use changes over long time, whereas the HI helps to quantify the human-felt temperature. Therefore, this is the reason for using both parameters. This study utilizes the land surface temperature (LST) obtained from the MODIS (Moderate Resolution Imaging Spectroradiometer) Aqua satellite sensor (MODIS/061/MYD11A1) from 2002 to 2022 for the summer months to assess the diurnal temporal variation in the land thermal parameters in urban areas. The MODIS Aqua sensor provides global LST measurements twice a day. The sun-synchronous orbits of the MODIS Aqua cross the equator at 13:30 and 01:30 (local solar time). The CORINE (Coordination of Information on the Environment) Land Cover dataset offers comprehensive data on land use and cover in Europe. It is crucial to monitor how land use is changing over time and recognize the rural and urban extent over the years. In addition, the air quality index datasets include the air quality index of particulate matters ($PM_{2.5}$ and PM_{10}), nitrogen dioxide (NO_2) and ozone (O_3) from various monitoring stations. These parameters are used to analyze the relation between the air quality and thermal stress. Further human-felt meteorological parameters like the air temperature at 2 m and relative humidity are extracted from Dexter. These measurements are utilized to calculate the heat index and quantify the human-felt temperature and humidity effects. The built-up settlement extents [41] provide information on the built-up areas and settlement extents, which is crucial for understanding urbanization patterns. Further, the population density and demographic data [42] are used to assess human exposure to thermal stress and air quality issues. The inclusion of vegetation as a criterion will help in providing valuable insights into the potential of vegetation-based solutions for mitigating the environmental stressors' impact. Therefore, the enhanced vegetation index (EVI) from 2002 to 2022 is used for long-term spatiotemporal vegetation trend analysis and hotspot mapping, whereas a local climate zone (LCZ) map [43] provides a detailed classification of the urban and natural land cover types to assess the impact of different urban forms on the local climate and thermal stress. In this study, it is used to quantify the vegetation ratio for sub-administrative risk ranking. Table 1 has detailed information on the datasets used for this study.

Table 1. Detailed information of dataset.

Dataset Used	Spatial Resolution	Time Period (Summer Months)	Source/Data Code
MODIS Aqua LST and Emissivity Daily Global	1 km	2002–2022	MODIS_061_MYD11A1
Copernicus CORINE Land Cover	100 m	2000, 2006, 2012, 2018	CORINE
Air Quality Parameters	Point station	2020–2022	AQICN
Meteorological Parameters (T2 and RH)	Point station	2020–2022	Dexter
Built Settlement Extents	100 m	2020	[41]
Population Demographics	100 m	2020	[42]
Aqua Vegetation Indices 16-Day	250 m	2002–2022	MODIS_061_MYD13Q1
LCZ	100 m	2018	[43]

3. Proposed Methodology

Figure 2 shows the proposed framework. In this study, a MCDA-based ERHMF is proposed to identify the risk hotspots based on environmental stress focusing on thermal conditions and air quality, the associated exposure and vulnerability and the existing vegetation status. Vegetation plays a critical role in modulating various environmental issues; therefore, vegetation-based criticality refers to the vegetation status and defines vegetation-based hotspot severity in the imminent future. In this context, the EVI was analyzed with each environmental criterion to enhance the understanding of the importance of vegetation in fostering urban resilience and facilitating the formulation of nature-based interventions. The risk assessment was carried out at a resolution of 1 km to maintain compatibility with the satellite-derived surface temperature, as it is considered as one of the major indicators of urbanization-led climate change. Further, a risk ranking approach for sub-administrative divisions was proposed, which involves quantifying environmental stressors and calculating the BGR (built-up green ratio: provides the vegetation status relative to the built-up areas) for each province. The detailed workflow is explained in the following subsections.

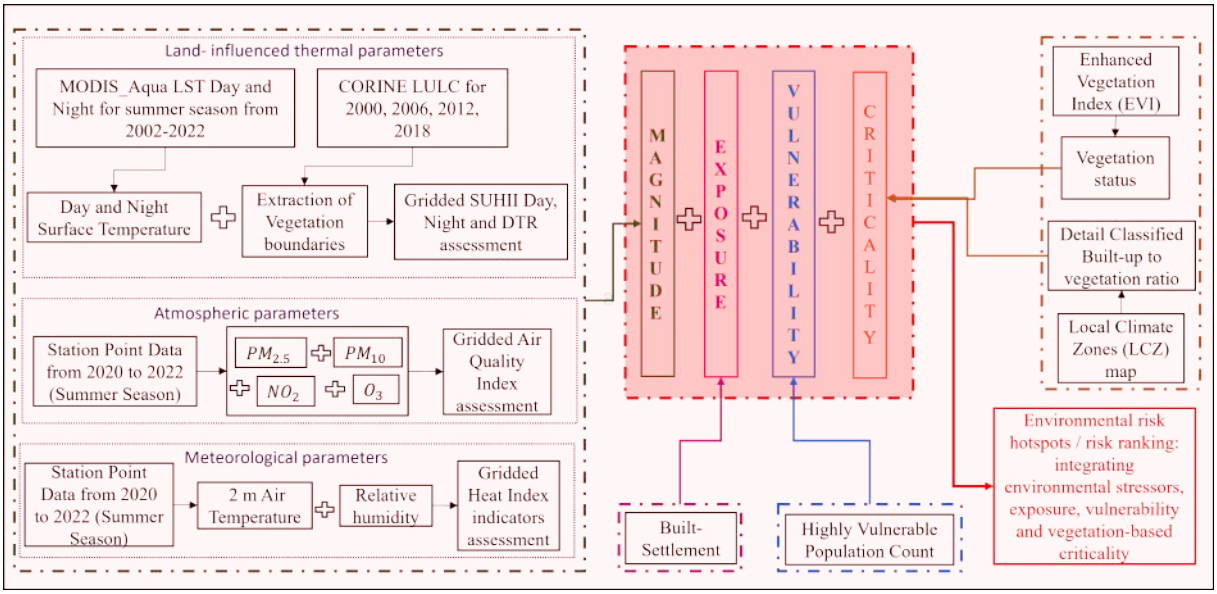

Figure 2. Workflow for ERHMF, where green dotted box consists of environmental stress magnitude criteria, pink dotted box with exposure parameter, light blue with vulnerability, brown with vegetation–based criticality for risk hotspots/risk ranking and red with final outcome: environmental risk hotspots.

3.1. Quantification of Environmental Stress Severity

Three of the major environmental parameters associated with the surface and atmosphere, which are the surface temperature, air quality and HI, are analyzed in this study. Analyzing the long-term SUHII using satellite-derived LST products was purposeful, as we aimed to perform a targeted assessment of the UHI phenomenon in response to evolving land use patterns [40]. The SUHII is a robust metric offering insights into the thermal properties of the surface, and the long-term focus on it allowed us to delve deeper into land use change-related effects. Furthermore, in a meteorological context, it is crucial to acknowledge the dynamic nature of variables like air temperature, relative humidity (RH) and air pollutant concentrations, as due to their dynamic nature they exhibit daily variations and possess a significant role in climatic studies over a broader context [44,45]. In addition, the HI and AQI data were derived from public weather stations, which have non-consistent and huge data gaps for historical records. Therefore, we considered a short-term analysis for the HI and AQI. However, to deal with temporal differences, the data were compiled based on the exponential weighted average (EWA) approach, prioritizing recent trends for all the parameters. The following subsections include a detailed explanation of the workflow for each environmental stress indicator.

3.1.1. Surface Thermal Trend

The surface thermal parameters associated with urban areas were analyzed by calculating the SUHII during the summer season for the years ranging from 2002 to 2022 using the MODIS LST data, by following the estimation of the temperature differentials between urban and rural areas following the approach described by [39,40]. The rural extent (excluding urban areas, water bodies and tree cover) was determined using the CORINE LULC (land use land cover) data for 2000, 2006, 2012 and 2018. For the estimation of the SUHII, the delineation of the rural boundaries for the years 2002–2005 was performed using the LULC of 2000; similarly for 2006–2011, the rural boundaries from the LULC of 2006 were used, and similarly, the rural boundaries from the 2012 and 2018 LULC were considered for the subsequent years. The resulting rural extent was used for calculating the average rural temperature, which was then subtracted from each pixel's temperature (Equation (1)). The procedure was repeated for the day and night LST data to obtain the respective SUHII at day and night. Additionally, the SUHII diurnal temperature difference was computed for each grid using the day and night SUHII values. Later, all the temporal SUHII indices or sub-criteria were compiled using the EWA, prioritizing recent trends while considering the time-series observations. Finally, these 21 years of data were combined into the respective SUHII indexes and extracted in a gridded format for further aggregating to identify the risk hotspot.

$$SUHII_i = LST_i - LST_{ruralarea} \quad (1)$$

where i is the pixel for which the SUHII is calculated.

3.1.2. Atmospheric Air Quality

The air quality was analyzed based on the AQIs representing four out of the other major air pollution components, i.e., $PM_{2.5}$, PM_{10}, NO_2 and O_3 (listed in Table 2), during the summer months from 2020 to 2022. Figure 1 shows the geographic location of the weather stations with blue dots. The spatial distribution of the AQI of these components was obtained by interpolating the weather station data using the IDW (inverse distance weighting) interpolation technique. Because of the IDW's adaptability in capturing local fluctuations without presuming an underlying statistical model, its ease of implementation and its efficacy with unequally distributed weather stations, we chose this interpolation method. The proximity-based weighting feature of the IDW guarantees precise local data representation, which is essential given the diverse geographic dispersion of our study. Further, it was extracted on a 1 km grid scale and temporally averaged using the EWA.

Table 2. The environmental parameters/indices used to compute the environmental stress magnitude, where the SUHII is the surface urban heat island intensity; DTR stands for diurnal temperature range; AQI stands for air quality index; HI is the heat index; and T_2 is the air temperature at a height of 2 m.

Parameter/Index	Description	AHP Assigned Weights
	Surface thermal parameters	
SUHII_Day	SUHII calculated using daytime LST	0.16
SUHII_Night	SUHII calculated using night-time LST	0.25
SUHII_DTR	Difference between SUHII_Day and SUHII_Night	0.59
	Air quality parameters	
AQI_PM2.5	AQI level of $PM_{2.5}$	0.56
AQI_PM10	AQI level of PM_{10}	0.11
AQI_NO2	AQI level of NO_2	0.05
AQI_O3	AQI level of O_3	0.28
	HI indicators	
HI_Avg	Average HI	0.07
HI_Max	Maximum HI in studied time period	0.06
Cum.HI_Intensity	Total HI intensity above threshold (HI > 27 °C)	0.28
Cum.HI_Frequency	Total days when HI was above threshold (≥27 °C)	0.46
Diff._T2 and HI	Difference between air temperature and HI	0.13

3.1.3. Computing Heat Index

In addition to the surface temperature, it is important to analyze the human-felt temperature in the environment. Therefore, the summer meteorological parameters retrieved from 2020 to 2022 include the air temperature at 2 m and the RH. Further, they were also interpolated using the IDW technique to obtain the spatial distribution of the T2 and RH. Following Equation (2) (source: https://www.wpc.ncep.noaa.gov/html/heatindex_equation.shtml (accessed on 15 November 2023)), the HI was calculated and extracted on a 1 km grid scale, which was further utilized to calculate the different indices (Table 2). Further, the T_2, the RH and all the indices computed based on the calculated HI were combined using the EWA concerning the temporal aspect.

$$\begin{aligned} HI_i = & -42.379 + 2.04901523 \times T_i + 10.14333127 \times RH_i \\ & - 0.22475541 \times T_i \times RH_i - 0.00683783 \times T_i \times T_i \\ & - 0.05481717 \times RH_i \times RH_i \\ & + 0.00122874 \times T_i \times T_i \times RH_i \\ & + 0.00085282 \times T_i \times RH_i \times RH_i \\ & - 0.00000199 \times T_i \times T_i \times RH_i \times RH_i \end{aligned} \quad (2)$$

where i is the pixel, HI is the heat index, T is the air temperature (°F) and RH is the relative humidity (%). Further, the averaged indices were normalized between 0 and 100 to attain uniformity for further analysis and were integrated using the AHP.

3.1.4. Analytic Hierarchy Process and Consistency Check

Each environmental stress criterion (surface temperature; HI; and air quality) was integrated by applying the analytic hierarchy process (AHP) at the sub-criteria level. For the integration of the environmental stress sub-parameters into the main stress criteria, a pairwise intensity importance matrix was created for each of them based on the ranking scale proposed by [46]. The pairwise intensity scores were also further referred to and

approved by the literature and domain experts, respectively. Further, the final weights were calculated based on the weighted average sum method. As the AHP is an additive and compensatory method, it is necessary to evaluate the consistency and robustness of the assigned weights. Therefore, to deal with the related uncertainties, the consistency ratio (CR) was calculated for each environmental stress criterion based on Equations (3) and (4). Following is an explanation of the calculation of the CR.

Let n be the number of criteria. After obtaining the pairwise comparison matrix A, where A_{ij} represents the score assigned for comparing criteria i with j, the consistency ratio was calculated as follows:

1. The weight vector w as the principal eigenvector of A was computed;
2. The consistency index (CI) using the formula

$$CI = \frac{\lambda_{\max} - n}{n - 1} \tag{3}$$

where $\lambda_{\max}$ is the maximum eigenvalue of A was computed;

3. The Random Index (RI) value corresponding to n was taken from the predefined table of RI values;
4. The consistency ratio (CR) as

$$CR = \frac{CI}{RI} \tag{4}$$

where (RI) is the Random Index value corresponding to n was calculated.

The CR indicates how consistent the pairwise comparison judgments are. Typically, if the CR is less than or equal to 0.1, the consistency is considered acceptable. Otherwise, the pairwise comparisons may need reviewing. The approach used to perform the consistency check for the calculated weights is the standard approach used while applying the AHP and which has been also used in other studies [29,30].

Finally, the three environmental stress parameters illustrating the SUHII, air quality and HI were aggregated with equal importance to produce the environmental stress magnitude map. They were given equal importance as each one of them can cause severe health-related risks when reaching their extremities, as exposure and vulnerability to either of them can be life-destructive. The spatial variability of the aggregated environmental stress magnitude was divided into 10 equal interval ranges (from 0 to 100) and grouped into 5 classes based on their stress intensity: none-to-negligible environmental stress (0–20), negligible-to-low stress (20–40), low-to-moderate stress (40–60), moderate-to-high stress (60–80) and high-to-extremely high stress (80–100).

3.2. Exposure and Vulnerability Analysis

The built-up settlement was used as an exposure indicator to risk and was retrieved at a 100 m resolution for the year 2020 (recent available year) and further extracted to a 1 km grid scale for the final hotspot mapping.

Vulnerability is related to fragility. Therefore, the population demographics describing the age structure of inhabitants in 2020 were retrieved at a resolution of 100 m. People with low immunity and less physical tolerance toward climate and weather extremes belong to the most vulnerable section of society based on their age. For this framework, children aged 5 years and below and elderly people aged 65 years and above were considered under this category, based on the experts' advice. Therefore, the total population count with this age structure in each grid area was considered for hotspot mapping.

3.3. Vegetation-Based Criticality Analysis

To comprehensively understand the relationship between vegetation and environmental stress, a multivariate correlation analysis was conducted. The analysis involved plotting a multivariate pairwise matrix, employing scatter plots and kernel density estimation (KDE) to examine the quantitative and qualitative distribution of data points for variables, such

as the EVI, SUHII, HI, AQI and CESM (Combined Environmental Stress Magnitude). The correlation coefficient quantified the pairwise linear relationship between these variables.

The LCZ scheme provides a valuable addition to the existing LULC, with a particular focus on urban and rural landscape types. The LCZ scheme comprises 17 distinct classes, each of which can be used to describe a unique type of environment. Among these classes, 10 are dedicated to describing the built environment, whereas a set of 7 natural land cover classes can be used as reference areas for a comparative analysis. Therefore, it offers a useful tool to investigate the relationships between urbanization, land cover and atmospheric conditions [43]. The LCZ map used in this study has a resolution of 100 m, offering detailed information about different urban and non-urban areas. For uniformity and a consistent hotspot analysis, we aggregated the LCZ types to a 1-kilometer grid size. This aggregation ensures that the analysis of environmental stress hotspots aligns with the resolution of other data layers used in our study. Here, the LCZ classification was used to calculate the BGR, i.e., the ratio of the total built-up area to the total vegetation area, to quantify the vegetation status for the risk ranking of sub-administrative divisions. It will also help to spatially analyze the environmental stress, typically over 10 built-up types.

3.4. Identification of Critical Environment Risk Hotspot and Ranking of Province

In our framework, the magnitude, exposure, vulnerability and vegetation-criticality were aggregated with equal importance to ensure a holistic assessment of environmental risks. Magnitude reflects climatic extremes and is weighted based on the literature and expert reviews, emphasizing the importance of climatic parameters. Exposure indicates the potential impact on human populations or assets, highlighting the need for equitable consideration in risk assessment. Vulnerability shows the susceptibility of communities, necessitating focused attention irrespective of magnitude. Vegetation-criticality underscores the role of green spaces in mitigating risks like urban heat islands and air pollution, influencing overall resilience. By giving equal weight to these factors, our approach ensures that all the critical dimensions of environmental stress are addressed, enabling a comprehensive and balanced identification of hotspots. This promotes effective risk mitigation and sustainable urban planning by integrating diverse aspects of environmental risk. The grids with higher intensity levels are highlighted as hotspot areas. Furthermore, to assign the environmental stress ranking, four criteria (i.e., the environmental stress magnitude, exposure, vulnerability and BGR) were quantified for each province based on the percentage area covered by each category score. As a larger built-up area over vegetation contributes positively toward environmental stress, accordingly, a higher score for risk ranking was given to the province with a higher built-up area with respect to its green area. Therefore, provinces with larger areas under high magnitude (80–100), large areas with built-up settlements, highly vulnerable populations and a high BGR were allotted higher scores. The province with the same ratio/area for either of these criteria was allotted the same score, and so on. Finally, the total score for each province was summed up to obtain the final score, assigning rank one to the province with the highest score. For the cases where provinces obtained the same total scores, the ranking was determined by prioritizing the higher score of risk criteria in the following order: stress magnitude, vulnerability, exposure and BGR.

4. Results and Discussions

This section focuses on the case study results obtained by applying the proposed ERHMF framework, with relevant discussions.

4.1. Consistency Check: Assigned Weights

A consistency check is essential in the AHP to understand the robustness and consistency of the decision-making outcomes concerning the deviation of the assigned weights from being consistent. As in this study, the combining of multiple parameters depends on

the spatial variability of the parameters as well as the weights assigned to them; it becomes primarily important to assess the robustness of the assigned weights.

It helps decision-makers make more robust and informed choices when dealing with complex decision problems by effectively evaluating how uncertainty in multiple input variables impacts the final weights. The pairwise matrix for each environmental stress criterion is explained in Figure 3, along with their computed CR, CI and RI values. The computed consistency ratio indicates that the weights assigned to the parameters are robust and consistent.

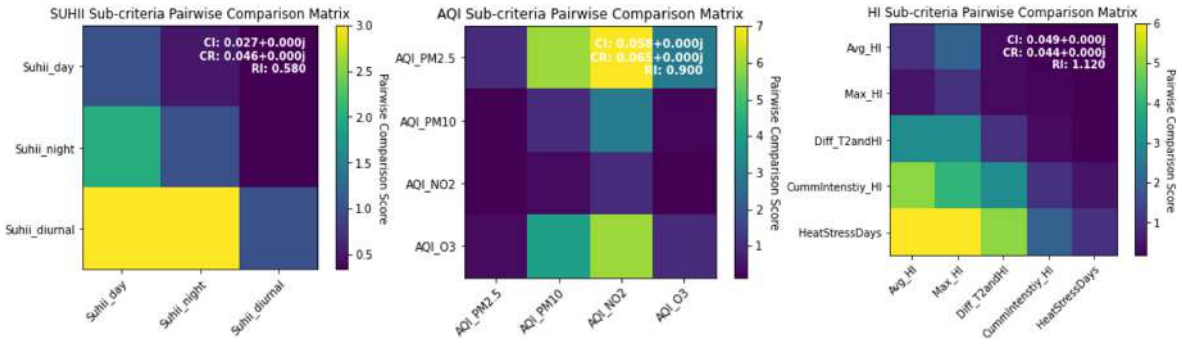

Figure 3. Pairwise matrix of each environmental stress parameter and their consistency check output.

4.2. Thermal and Air Quality-Based Environmental Stress Magnitude

The systematic and detailed analysis of the environmental stress parameters was performed by categorizing them based on different criteria, primarily focusing on their intensity and/or frequency in the course of the temporal investigation. Analyzing the SUHII trend over a long period is necessary to accurately understand and assess changes in surface thermal stress, as it is impacted by long-term land use changes and urbanization processes [47]. The long-term trends of the SUHII also indicate the climate change impacts, showing the persistent increase in surface temperatures due to global warming. This sustained thermal stress in urban areas correlates with broader climatic shifts, underscoring the essential impact of climate change on urban environments. Variations in the concentration of different air components and weather patterns are a function of a short-time period [44,45]. Therefore, in this study, the AQI and HI analyzed for recent years (short-term period) provided an evaluation of the latest state of the air quality and human-perceived thermal stress. This unique dual approach, the long-term analysis of the SUHII and short-term analysis of the AQI and HI, allowed us to comprehensively capture both enduring and immediate environmental stressors. By integrating these temporal scales, our framework effectively delineated the impact of climate change on urban thermal stress while also addressing more immediate atmospheric conditions and their effects on urban livability.

4.2.1. Surface Urban Heat Island Intensity Analysis

The surface urban heat island intensity (SUHII) indicators are mapped in a blue-to-red color ramp, indicating lower to higher levels of intensity (Figure 4). The spatial distribution of the cumulative $SUHII_{day}$ shows that water bodies remained cool, while built-up areas exhibited higher temperatures compared to the surrounding vegetation (Figure 4a). The SUHII during a summer day in 2002 was 4.87 °C, which increased to 6.19 °C in 2021 and 5.97 °C in 2022 as indicated in the yearly trend graph in Figure 4a. The $SUHII_{night}$ is a more appropriate indicator for distinguishing built-up areas, as it considers the heat emission phenomenon of built-up areas at night. The $SUHII_{night}$ decreased over the years, quantitatively measuring 1.53 °C in 2002 and subsequently declining to 0.81 °C in 2021 and 0.75 °C in 2022 (Figure 4b). These changes have subsequently impacted the $SUHII_{diurnal}$ variation over time, which increased from 3.09 °C in 2002 to 5.04 °C in 2021 and 4.82 °C in

2022 (Figure 4c). The graphs in Figure 4 clearly explain the increasing trend observed over the yearly time period for each SUHII indicator.

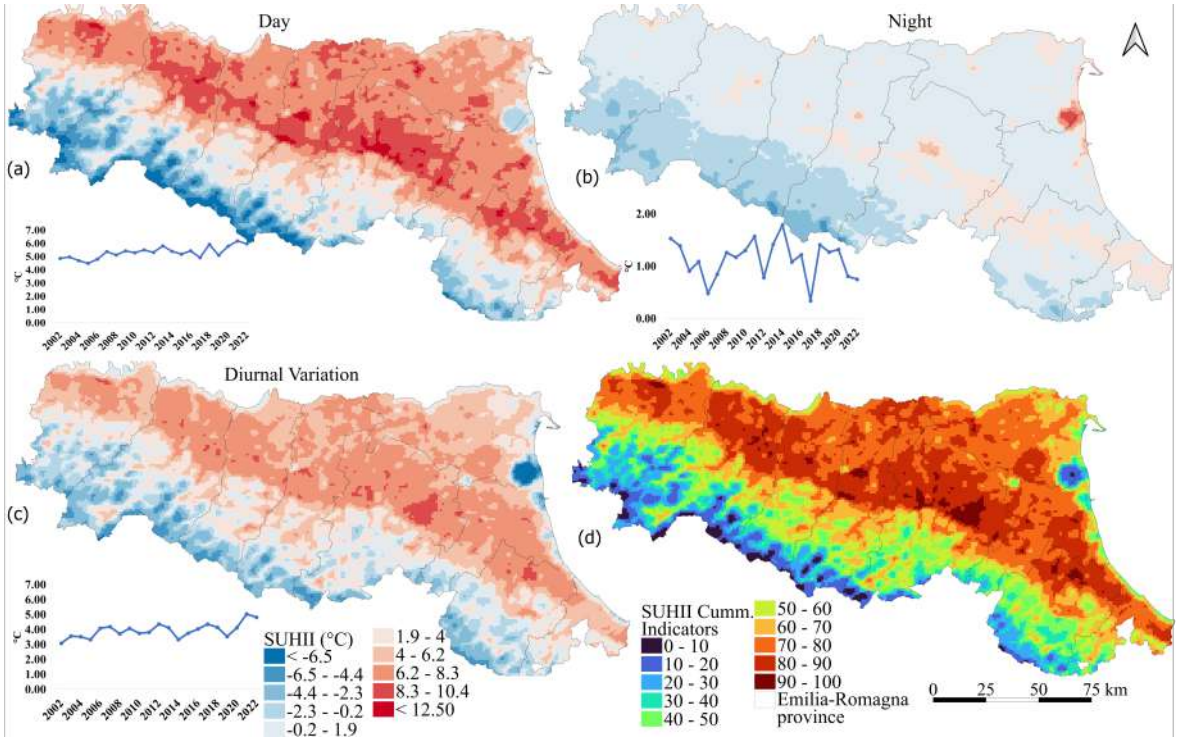

Figure 4. The SUHII indicators showing the cumulative spatial variability and yearly mean of the (**a**) $SUHII_{Day}$, (**b**) $SUHII_{Night}$, and (**c**) $SUHII_{Diurnalvariation}$ for the summer months from 2002 to 2022 and (**d**) the cumulative SUHII indicators combining (**a**–**c**). The graph with each SUHII indicator map represents the yearly mean trend between 2002 and 2022 for the respective indicator. The SUHII legend with (**c**) represents the legend for (**a**–**c**).

Despite the agricultural dominance in the ER region [37], the long-term SUHII trend (Figure 4) reveals higher thermal intensities during the daytime in urban and agricultural areas due to climate change and urbanization. This is likely influenced by increasing urbanization and agricultural land abandonment caused by rural-to-urban migrations. Conversely, at night when the UHI effect is prominent, the SUHII is significantly higher in built-up areas and urban sprawls (Figure 4b). Higher SUHII diurnal differences can pose several risks to urban health with varied danger potentials due to the extreme fluctuation in temperature differences during the day and night. The first one to list is (a) increased heat-related health risks: a higher SUHII diurnal difference is the result of a significant temperature contrast between urban and rural areas, which might result in heat exhaustion, heatstroke and other heat-related illnesses being more prevalent among the vulnerable populations [48,49]. Then, (b) increased energy demand/consumption: with the increased SUHII diurnal difference, the UHI effect also intensifies leading to increased energy demand for cooling, straining urban infrastructure like power grids, which contributes to increasing the greenhouse gas emissions [9]. And finally, (c) reduced air quality: the formation of pollutants worsening the air quality is being promoted by increased urban temperatures; therefore, stagnant air conditions and increased energy consumption together may result in increased ground-level ozone and other harmful pollutants, impacting the respiratory health of people [44,50]. Combining these three indicators gives the overall distribution of the surface thermal stress (Figure 4d). Based on the spatiotemporal trend, the northern and northeastern regions witnessed higher stress, which declined toward the south–west of the ER region.

4.2.2. Air Quality Index (AQI) Assessment

The major air quality components studied include $PM_{2.5}$, PM_{10}, NO_2, O_3, SO_2, CO, etc. The current framework analyzed the AQI of the $PM_{2.5}$, PM_{10}, NO_2 and O_3 specifically during the summer months of recent years (2020–2022). Each component of the AQI has its range of values, while the color ramp used in Figure 5a–d ranges from green (lower concentration levels) to red (higher concentration levels).

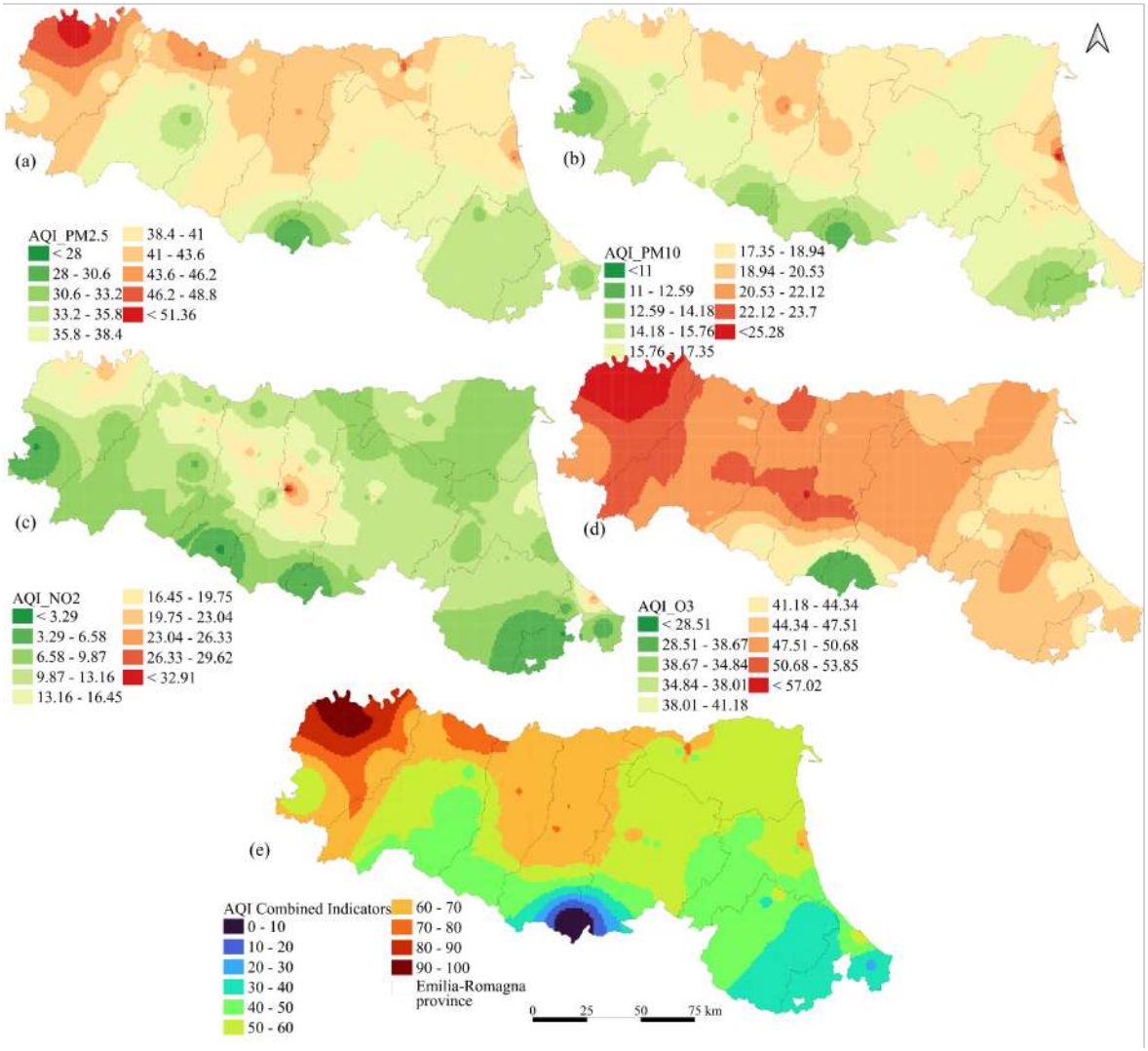

Figure 5. Cumulative spatial variability of (**a**) $AQI_{PM2.5}$, (**b**) AQI_{PM10}, (**c**) AQI_{NO2} and (**d**) AQI_{O3} for summer months from year 2020 to 2022; (**e**) AQI spatial variability combining (**a**–**d**).

The spatial distribution of the temporal cumulative $AQI_{PM_{2.5}}$ (Figure 5a) indicates a major part of Piacenza and Modena, while a smaller area of Ravenna is experiencing higher concentrations of $PM_{2.5}$. The distribution of the $AQI_{PM_{10}}$ (Figure 5b) shows higher concentrations in certain parts of Ravenna, whereas a high AQI_{NO_2} (Figure 5c) is observed over the Modena province. In addition, the AQI_{O_3} (Figure 5d) exhibits higher and moderate concentration levels distributed across almost all provinces, covering a significant portion of their respective area. This distribution varies according to the landscape settings, as topography plays an important role in the air quality along with impacting temperature, as healthy vegetation and hilly landforms contribute to the purification of the surrounding atmosphere [51]. Therefore, Bologna, on average, witnesses cleaner air with a low cumulative AQI ((Figure 5e), where the blue to red color ramp depicts the cleaner to polluted air quality), over the studied temporal course, probably because of its higher elevation

and proximity to the hilly areas. In addition, Forli'-Cesena, parts of Rimini, Ravenna, the southern parts of Parma, the southernmost area of Reggio nell'Emilia and Modena also show good air quality. Therefore, evaluating the cumulative AQI by combining the major AQI components, weighted according to their relative environmental risk, offers significant value to urban climate research. This approach, rather than assessing individual AQI components separately, highlights areas with high concentrations of multiple air pollutants, aiding in the planning and development of sustainable living environments.

The analysis of the SUHII and AQI distribution reveals an important finding. As the SUHII and its diurnal difference increase (Figure 4), there is a corresponding rise in the ozone concentration (Figure 5). This finding aligns with another recent study conducted by [24], which established the synergy between air pollution and urban heat by emphasizing a causal correlation between them through a detailed literature review and experimental investigations.

4.2.3. Heat Index Analysis

The HI is a commonly used metric to quantify the thermal stress experienced by the human body under specific temperature and RH conditions. In the ER region, the average air temperature during the summer months in 2020, 2021 and 2022 was recorded as 21.98 °C, 22.70 °C and 23.71 °C, respectively. Concurrently, the average RH was measured as 60.56%, 54.67% and 54.33%, respectively. Therefore, the calculated average HI was found to be 24.13 °C, 24.36 °C and 24.77 °C, respectively.

Figure 6 depicts the spatial distribution of the variables utilized in the computation of the HI and other derived indices. The spatial pattern of the air temperature (Figure 6a) reveals significant variations, with the highest values observed in Piacenza, Reggio nell'Emilia and Bologna. Conversely, the RH (Figure 6b) exhibits elevated levels in substantial areas of Ferrara, the southern region of Reggio nell'Emilia and Bologna.

The cumulative average HI (Figure 6c) for the ER region surpasses 20 °C, while a large extent of Ferrara has a maximum HI (Figure 6d), followed by Bologna, Parma and Piacenza. The Bologna province records the highest number of cumulative HI days (days with the HI $\geq$ 27 °C; Figure 6e) and a greater cumulative intensity of heat stress (intensity above 27 °C; Figure 6f). The majority of the area witnesses a range of 1–1.8 °C difference between the air temperature and HI (Figure 6g). Moving from north to south, this difference increases, indicating higher humidity levels. The city centers of the major cities exhibit lower differences and RH levels.

It is noteworthy that regions in proximity to water bodies exhibit higher RH but lower air temperature, resulting in lower average HI values. Conversely, land surfaces distant from water sources exhibit lower RH and a higher temperature, placing them within the caution level range of the HI ($\geq$27 °C) according to the HI look-up table (source: https://www.weather.gov/ffc/hichart (accessed on 15 November 2023)). The elevated intensity and frequency of the caution-level HI values emphasize the associated risk of heightened thermal stress, as prolonged exposure to elevated temperatures poses greater danger as suggested by the heat index documentation (source: https://www.noaa.gov/jetstream/global/heat-index (accessed on 15 November 2023)). Figure 6h illustrates the spatial variability of the combined HI derivatives (Figure 6c–g), categorized into ten equal intervals, highlighting the area with a higher HI (with red color gradient).

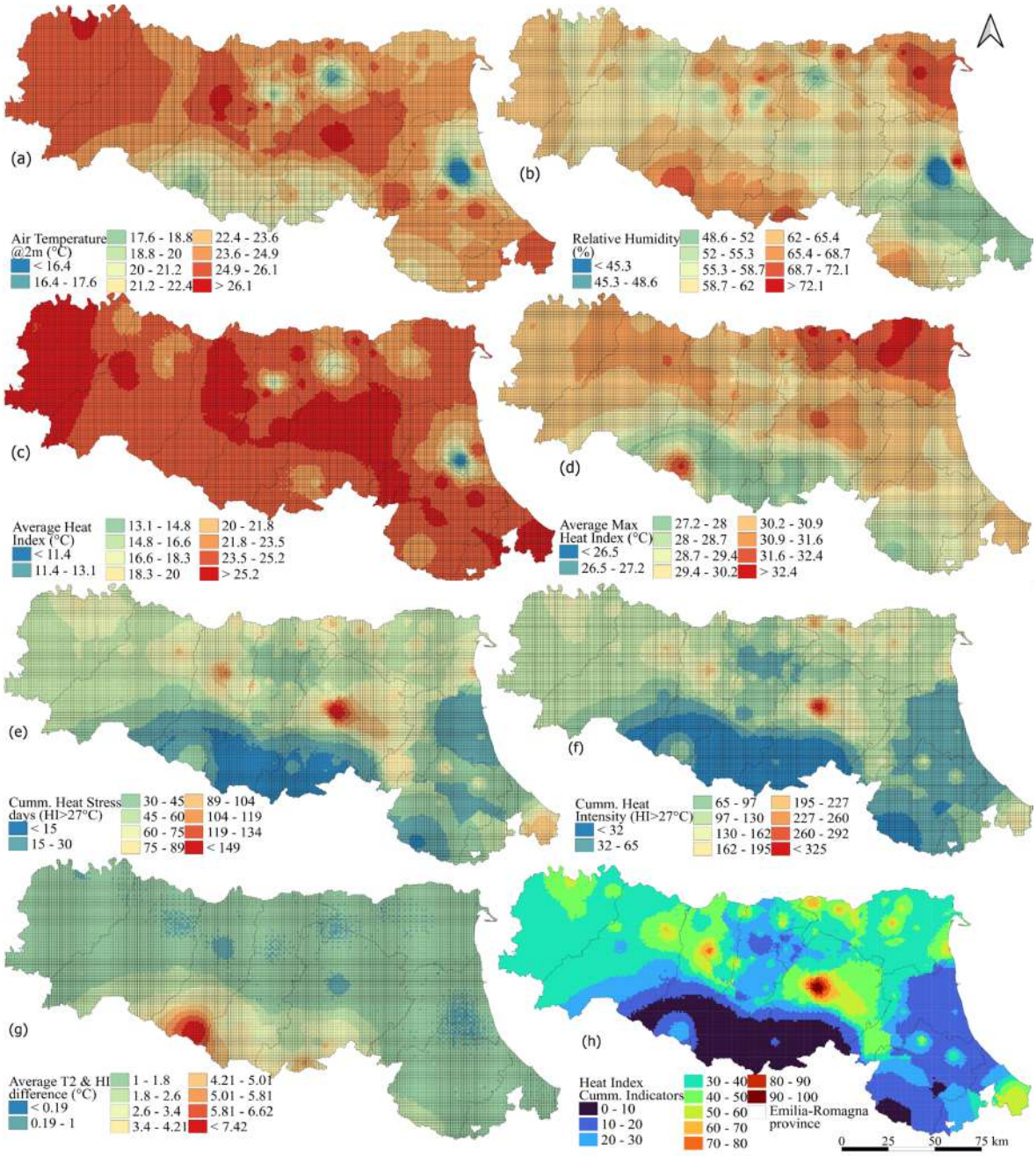

Figure 6. Cumulative spatial variability of (**a**) air temperature at 2 m, (**b**) RH, (**c**) average HI, (**d**) average of max HI, (**e**) cumulative heat stress days (with HI $>$ 27 °C), (**f**) cumulative HI intensity (HI $>$ 27 °C) and (**g**) average difference between T2 and HI for the summer months from 2020 to 2022; (**h**) cumulative HI indicators combining (**c**–**g**).

4.3. EVI and Its Correlation with Environment-Risk Magnitude Variables

The relationship between the cumulative EVI and magnitudes of environmental stress was analyzed using a pairwise correlation analysis. Figure 7 represents the scatter plot (depicting data points as dots on a plot, with one variable on the x-axis and the other on the y-axis), correlation coefficient (ranging from -1 to +1) and trend line of the relation between each pair of variables in its upper right triangle. The correlation coefficient range indicates the direction and strength of the linear relationship between the variables, with the p-value < 0.05. Moreover, the lower left triangle exhibits the KDE plots, a smoothed distribution of the variable, which provide insights into its shape and pattern for each pair

of variables. This color scheme of the KDE plots facilitates the visualization of areas with high (yellow) and low (blue) data point concentrations within the variable's distribution.

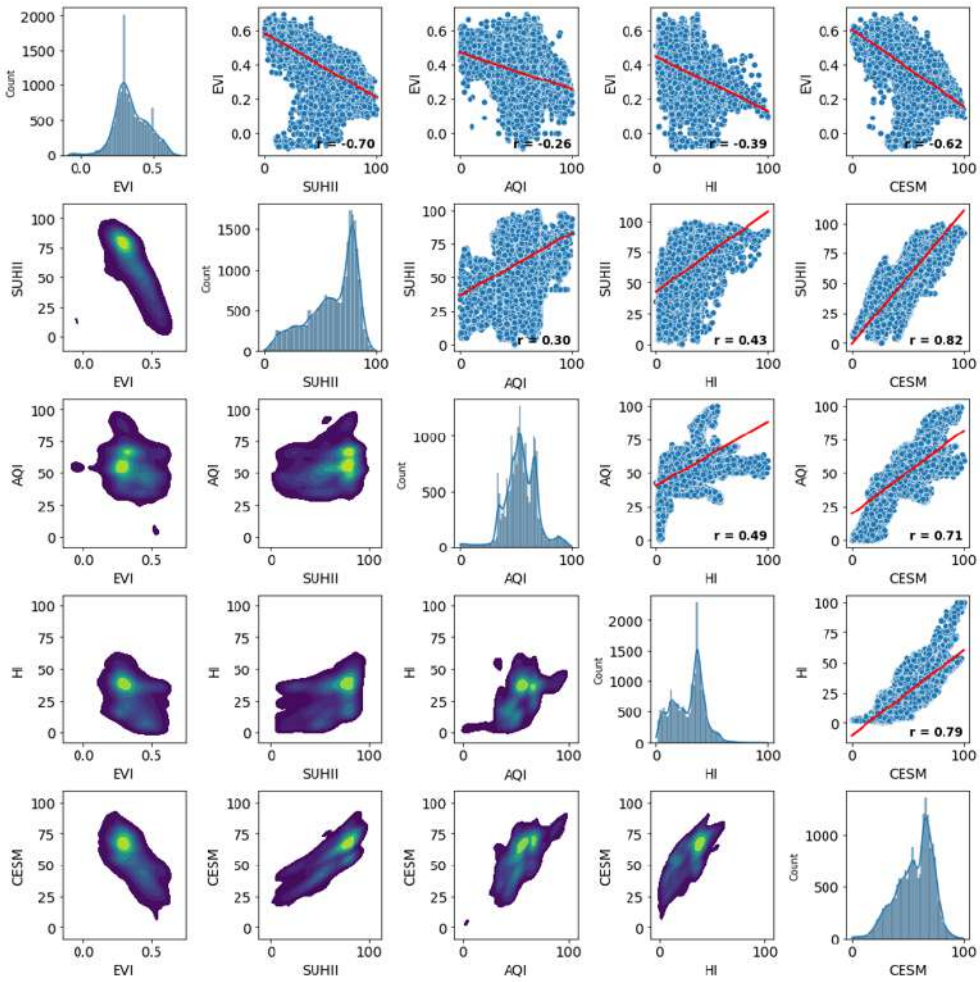

Figure 7. The multivariate pairwise distribution and scatter plot matrix of the environmental stress magnitude parameters, where the upper right triangle consists of the scatter plot, correlation coefficient and trend line; the lower left triangle represents the KDE plot The color scheme of KDE plot shows the higher (yellow color) to lower (blue color) data points' concentration within the variable's distribution. The SUHII, AQI, HI and CESM are normalized between 0 and 100, whereas the EVI is between -1 and 1. The plots are significant with a p-value < 0.05.

A strong negative correlation ($r = -0.7$) is observed between the cumulative SUHII and EVI, indicating that the area with a higher SUHII has limited healthy vegetation, negatively impacting the micro- and macroenvironment [52,53]. Urban expansions and sprawls result in the inadequate maintenance of urban green spaces within built-up areas and their surroundings, leading to increased exposure to heat-related risks, as evidenced by the higher data point density observed in regions with a high SUHII and low EVI (Figure 7). Additionally, rural-to-urban migration and the subsequent agricultural land abandonment contribute to the rising temperature and other environmental stresses, further exacerbating the situation. The AQI showed a weak negative correlation with the EVI ($r = -0.26$), with a higher data density at moderately high AQI levels and low EVI values. This suggests that urban areas need dense vegetation for the mitigation of environmental stress caused by a high SUHII and AQI, and similar suggestions have been made in recent studies [54,55].

However, it is noteworthy that analyzing the KDE plots of separate indicators and combined magnitude with the EVI leads to an interesting observation. At similar EVI data density points, the HI is comparatively lower than the SUHII, AI and CESM, which indicates

that even sparse vegetation can have a considerable impact in moderating the atmospheric thermal stress, probably because of cooling procedures, like evapotranspiration. This inference can also be analyzed and compared among other climatic conditions in future studies to result in a more robust conclusion. The density distribution patterns, scatter plots and correlation coefficients provided quantitative and qualitative insights, thus aiding the independent analysis and assessment of various environmental stress parameters with vegetation status and further enabling a deeper exploration of the relationships and the formulation of more suitable solutions for environmental stress mitigation measures.

4.4. Cumulative Environmental Stress Magnitude, Settlement Exposure, Population Vulnerability and Vegetation-Based Criticality

The integration of the SUHII, AQI and HI indicators has yielded a measure of the magnitude of environmental stress. The read spatial distribution of this environmental stress magnitude (Figure 8A(a)) reveals a significant area of Piacenza, Bologna and Reggio nell'Emilia experiencing high-to-extremely high stress levels (80–100). Parts of Parma, Modena and Ferrara fall within the moderate-to-high stress range (60–80). Ravenna and Rimini have relatively smaller areas classified as moderate-to-high stress, while Forli'-Cesena is predominantly characterized by low-to-moderate (40–60) and negligible-to-low (20–40) stress levels. The quantitative distribution has been demonstrated in Figure 8B(a), highlighting the relative percentage area covered by each stress magnitude range in the respective province.

The assessment of risk exposure focuses on built-up settlements, as they constitute primary habitation for most of the human population and contribute significantly to the amplification of existing thermal and environmental stress factors [40]. Figure 8A(b) shows the highest environmental stress exposure in Bologna, followed by Modena, Reggio nell'Emilia, Ferrara, Ravenna, Parma, Forli-Cesena, Rimini and Piacenza. This hierarchy reflects the extent and density of the built-up settlements in these areas. The vulnerability mapping (Figure 8A(c)) identifies the population that is most sensitive to environmental stress. The LCZ mapping (Figure 8A(d)) illustrates that the northern, central, northwestern, northeastern and eastern parts of the region are predominantly covered by low plants, while the southern, southwestern and southeastern areas have dense and scattered trees. This spatial differentiation in vegetation cover is crucial for understanding regional variations in microclimatic conditions. The urban areas across each province exhibit varied land use classes. The built-up patterns observed in the major cities of the ER region indicate the concentration of compact midrise and compact lowrise buildings in the center, surrounded by open midrise and open lowrise structures. Large lowrise built-up areas are located toward the outer periphery. Sparse industrial areas are mainly found in eastern Bologna, southern Ravenna and the central and northern parts of Forli'-Cesena and Rimini. This distribution pattern highlights the varied urban morphology and its implications for environmental stress. The cumulative vegetation distribution (Figure 8A(e)) shows the area with insufficient green coverage, as evidenced by the low values of the EVI. The presence of water is signified by an EVI < 0, built-up and bare land < 2 and low plants and agricultural land by an EVI < 4, while green and healthy vegetation is shown by an EVI < 4 [56]. This vegetation analysis is pivotal for identifying areas lacking adequate greenery and the increasing proportion of impermeable surfaces, which exacerbate thermal stress and reduce resilience to environmental changes. Figure 8B represents the quantitative distribution of different legend classes of the respective parameters illustrated in Figure 8A(a–e), offering a comprehensive overview of the spatial and quantitative variations in the environmental stress factors, built-up areas, vegetation cover and land use classes across the ER region. This detailed mapping and analysis facilitate a better understanding of the interplay between urban morphology, vegetation distribution and environmental stress, thereby aiding in the formulation of effective mitigation strategies.

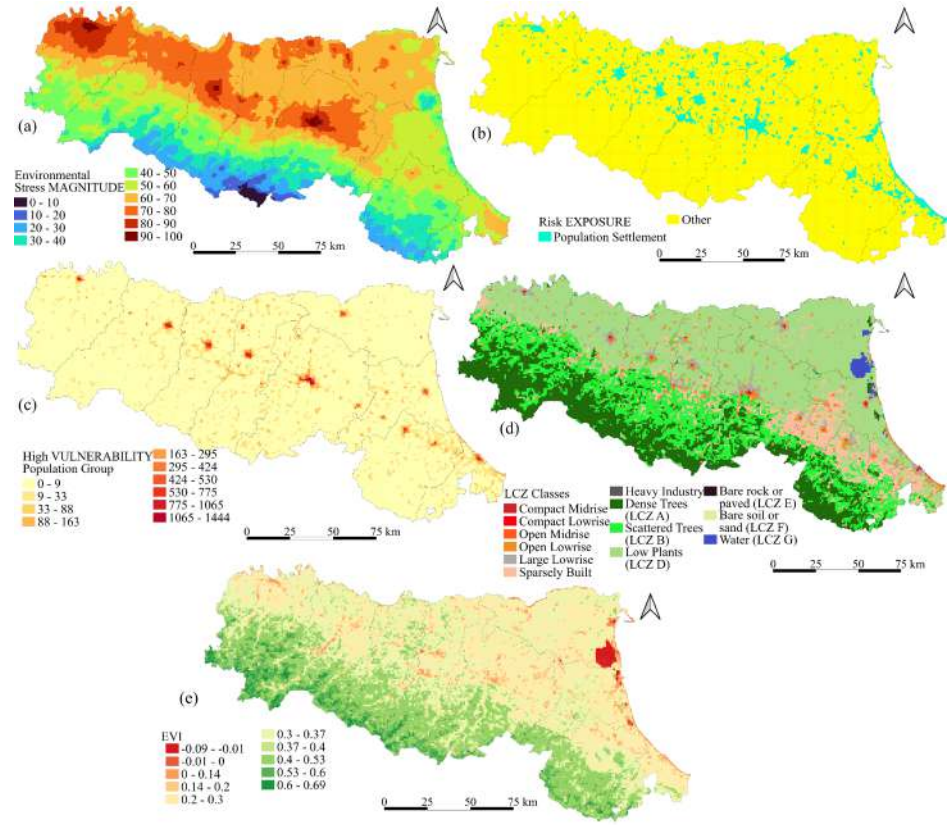

(**A**)

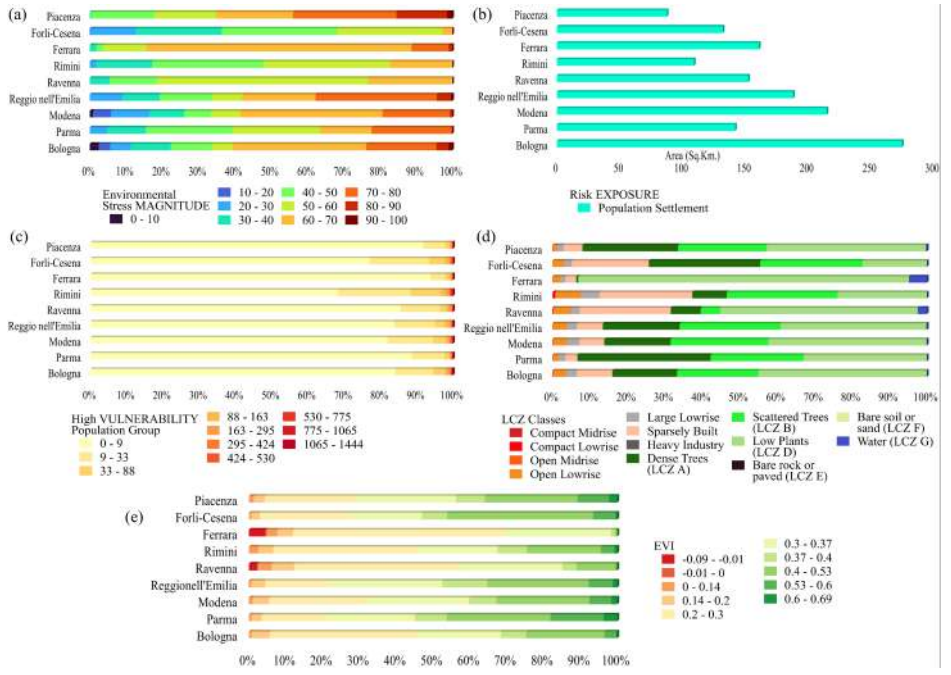

(**B**)

Figure 8. (**A**): (**a**) The environmental stress magnitude combining the cumulative SUHII, AQI and HI; (**b**) the population density at 1 km showing the exposure levels; (**c**) the high vulnerable population class at 1 km; the vegetation–based criticality in the form of (**d**) LCZ classes showing the spatial distribution of the LULC for the risk ranking; and (**e**) the EVI showing the spatial vegetation status for the hotspot mapping. (**B**): The graphs (**a**–**e**) correspond to each map (**A**) showing the province–wise quantitative distribution of the legend classes of the respective maps.

4.5. Risk Hotspot Mapping and Province Ranking

Figure 9a demonstrates the combination of the environmental stress magnitude, exposure, vulnerability and EVI. Most grids with higher magnitudes (80–100 range) are concentrated in the Bologna province, while Modena and Piacenza exhibit very few grids within this range. The spatial distribution of these hotspots is discernible in Figure 9a, while Figure 9c demonstrates the quantitative distribution of the relative percent area of each province under different environmental stress levels. It shows that a total of a 6,000,000 m^2 area of Bologna is witnessing high-to-extremely high stress (80–100) based on the recent environmental stress criteria. However, the areas under the moderate-to-high stress range (60–80) for Bologna, Reggio nell'Emilia, Modena, Parma, Piacenza, Ferrara and Rimini are 12,000,000 m^2, 7,000,000 m^2, 5,000,000 m^2, 5,000,000 m^2, 4,000,000 m^2, 2,000,000 m^2 and 1,000,000 m^2, respectively.

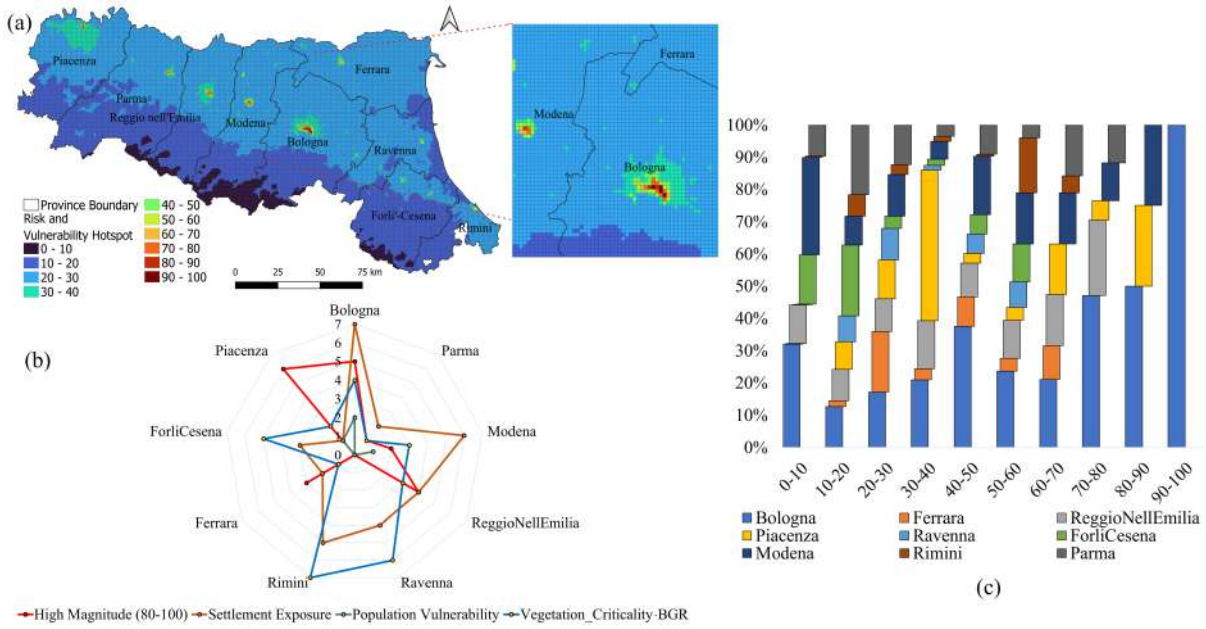

Figure 9. (**a**) Spatial distribution of identified environmental risk hotspots; (**b**) risk ranking for sub ER provinces; and (**c**) quantitative area distribution chart showing relative percentage area covered by each environmental stress range in different provinces.

Table 3 contains the quantitative score for each province based on individual criteria, explaining the provincial-level quantitative evaluation. It shows Piacenza exhibits a higher relative percentage area under stress magnitude; on the contrary, Bologna has a greater concentration of settlements with higher exposure and vulnerable populations compared to other provinces. This underscores Bologna's significant risk due to its dense population and extensive urbanization. Furthermore, Rimini demonstrates the highest built-up-to-green ratio, earning the highest score for the BGR. This high ratio signifies a critical lack of green spaces relative to built-up areas, exacerbating the environmental stress due to limited vegetation cover that can mitigate urban heat island effects and other stressors. Combining the scores from all four assessed criteria for ranking (Figure 9b), Bologna emerges as the province with the highest overall risk. This comprehensive ranking takes into account factors, such as the stress magnitude, exposure, vulnerability and built-up-to-green ratio. On the other hand, Parma ranks at the bottom, indicating the lowest overall risk among the provinces studied. The remaining provinces fall in between, with the descending order of risk and vulnerability as follows: Modena > Rimini > Reggio nell'Emilia > Piacenza > Ravenna > Forli-Cesena > Ferrara. This gradient highlights the varying degrees of environmental and thermal stress across the region, reflecting differences in urbanization patterns, vegetation cover and population distribution. This comprehensive

ranking assessment offers valuable insights for policymakers and urban planners. It ranks critical areas at the sub-administrative level where interventions are needed to reduce environmental stress and enhance resilience. By focusing on high-risk areas, targeted strategies can be developed to increase green spaces, improve urban planning and reduce exposure and vulnerability to environmental stressors.

Table 3. The risk ranking for the ER provinces based on the relative percentage area covered by the high-risk magnitude range (80–100); settlement percentage area; total vulnerable people; and built-up–green ratio depicted by the BGR.

Risk Parameters	Bologna	Parma	Modena	ReggioNellEmilia	Ravenna	Rimini	Ferrara	ForliCesena	Piacenza
High Magnitude (80–100)	5	1	2	4	0	0	3	0	6
Settlement Exposure	7	2	6	4	4	5	2	3	1
Population Vulnerability	2	0	1	0	0	0	0	0	1
Vegetation_Criticality (BGR)	4	1	3	3	6	7	1	5	2
Total score	**18**	**4**	**12**	**11**	**10**	**12**	**6**	**8**	**10**

5. Conclusions

This study presents an ERHMF, based on multiple environmental stressors, focusing on thermal and air quality parameters consisting of the SUHII, HI and AQI for highlighting the risk hotspots. To evaluate these parameters from multiple aspects, several indices have been designed and computed for each parameter, which were later combined using the popularly known methodological aspect called MCDA in integration with GIS, at the grid resolution of 1 km. It is important to note that this framework analyzes both short- and long-term temporal data based on the efficacy of the used parameters. Moreover, exponential weighted aggregation being capable of effectively capturing trends, handling noise and outliers and adapting to changing dynamics provided more accurate outputs, which helped in understanding the underlying patterns and making informed decisions based on up-to-date information. The less explored approach of applying the AHP on the sub-criteria level to obtain the main risk criteria has led to the results capturing a more detailed spatial distribution and percentage area covered by the environmental stress magnitude in each province. Because of this, the framework approach has succeeded in accurately capturing the cumulative risk associated with each criterion. For example, for the surface thermal stress, the cumulative risk layer represents the area with higher risk considering the importance of all the used indices, that is, the surface thermal stress during the day and during the night and the diurnal difference. Similarly, the human-felt thermal stress and air quality-related stress have resulted in the compact and confined distribution of the stress levels because of the consideration of the maximum possible indices and variables covering multiple aspects.

The correlation analysis between the magnitude of environmental stress criteria and vegetation has provided valuable insights into the pairwise relationships between the EVI, SUHII, HI, AQI and CESM. The vegetation status analysis has emphasized its critical role in determining environmental risk. Furthermore, including the LCZ classification-based vegetation fraction has resulted in a more accurate ratio of built-up and vegetation areas, as the LCZ is a detailed classification for natural as well as paved surfaces, typically urban buildings. This would help in better understanding and the implementation of the green mitigation measures for risk hotspots.

Therefore, this framework is capable of capturing the cumulative risks, considering the sub-criteria level to avoid the chance of missing out on considering any kind of risk probability. Hence, it will aid policymakers and planners in evaluating and identifying major environmental risk-exposed areas. The proposed risk ranking system for administrative subdivisions will enable the listing based on risk hierarchy, facilitating mitigation planning. The hotspot analysis identifies locations in need of vegetation coverage, allowing for targeted interventions such as urban parks, green buildings, green roofs, etc., based on LULC considerations.

Future Work

This framework aids in identifying hotspots that require urgent mitigation measures for the risk criteria. Based on findings at the regional scale, further developments can allow for assessing neighborhood-level impacts at a microclimate scale: the proposed ERHMF can be utilized to map environmental risk hotspots at the city scale based on the availability of high-resolution data. Moreover, the correlation between vegetation and environmental stress criteria has been examined within a specific climate type, warranting further investigation on a global scale to understand this relationship across different climate types.

Author Contributions: Conceived and designed the experiments, P.R. and D.T.; experimentation and data analysis, P.R.; first draft, P.R.; funding acquisition, P.T.; revised draft: P.R., D.T. and P.T. All authors have read and agreed to the published version of the manuscript.

Funding: The research has been carried out within the PhD project "Big data and "healthy cities": regeneration of urban contexts, green systems and safe and healthy lifestyles", funded by the Emilia-Romagna Region (Italy) within the Research training projects "Big Data per una regione europea più ecologica, digitale e resiliente" (Fondo POR FSE—Resolution n. 752 of 24 May 2021).

Data Availability Statement: Open-source and freely available datasets have been used, and the references to respective sources are mentioned in the data used section. Further details will be made available on request.

Acknowledgments: The authors would like to thank experts Stefania Toselli, in Anthropology at the Department for Life Quality Studies, and the researchers of the Biosystems Engineering lab, of the University of Bologna, for their kind participation in the expert discussion that has contributed to assigning the importance of the variables, considering the health-related aspects of environmental stress factors.

Conflicts of Interest: The authors declare no conflicts of interest.

References

1. Liu, B.; Song, W.; Sun, Q. Status, Trend, and Prospect of Global Farmland Abandonment Research: A Bibliometric Analysis. *Int. J. Environ. Res. Public Health* **2022**, *19*, 16007. [CrossRef]
2. Pawlewicz, A.; Pawlewicz, K. The Risk of Agricultural Land Abandonment as a Socioeconomic Challenge for the Development of Agriculture in the European Union. *Sustainability* **2023**, *15*, 3233. [CrossRef]
3. EU. *Report from the Commission to the European Parliament, the Council, the European Economic and Social Committee and the Committee of the Regions*; Working paper; European Union: Maastricht, The Netherlands, 2023.
4. Vizzari, M.; Hilal, M.; Sigura, M.; Antognelli, S.; Joly, D. Urban-rural-natural gradient analysis with CORINE data: An application to the metropolitan France. *Landsc. Urban Plan.* **2018**, *171*, 18–29. [CrossRef]
5. Galan, J.; Galiana, F.; Kotze, D.J.; Lynch, K.; Torreggiani, D.; Pedroli, B. Landscape adaptation to climate change: Local networks, social learning and co-creation processes for adaptive planning. *Glob. Environ. Chang.* **2023**, *78*, 102627. [CrossRef]
6. Rao, P.; Tassinari, P.; Torreggiani, D. Exploring the land-use urban heat island nexus under climate change conditions using machine learning approach: A spatio-temporal analysis of remotely sensed data. *Heliyon* **2023**, *9*, e18423. [CrossRef]
7. Kalisa, E.; Fadlallah, S.; Amani, M.; Nahayo, L.; Habiyaremye, G. Temperature and air pollution relationship during heatwaves in Birmingham, UK. *Sustain. Cities Soc.* **2018**, *43*, 111–120. [CrossRef]
8. Wu, J.; Zheng, H.; Zhe, F.; Xie, W.; Song, J. Study on the relationship between urbanization and fine particulate matter (PM2.5) concentration and its implication in China. *J. Clean. Prod.* **2018**, *182*, 872–882. [CrossRef]
9. Bibri, S.E.; Krogstie, J. Smart sustainable cities of the future: An extensive interdisciplinary literature review. *Sustain. Cities Soc.* **2017**, *31*, 183–212. [CrossRef]
10. Piracha, A.; Chaudhary, M.T. Urban air pollution, urban heat island and human health: A review of the literature. *Sustainability* **2022**, *14*, 9234. [CrossRef]
11. Heaviside, C.; Vardoulakis, S.; Cai, X.M. Attribution of mortality to the urban heat island during heatwaves in the West Midlands, UK. *Environ. Health* **2016**, *15*, 49–59. [CrossRef]
12. Jabbar, H.K.; Hamoodi, M.N.; Al-Hameedawi, A.N. Urban heat islands: A review of contributing factors, effects and data. In *Proceedings of the IOP Conference Series: Earth and Environmental Science*; IOP Publishing: Bristol, UK, 2023; Volume 1129, p. 012038.
13. Mirzaei, P.A. Recent challenges in modeling of urban heat island. *Sustain. Cities Soc.* **2015**, *19*, 200–206. [CrossRef]
14. Analitis, A.; Michelozzi, P.; D'Ippoliti, D.; de'Donato, F.; Menne, B.; Matthies, F.; Atkinson, R.W.; Iñiguez, C.; Basagaña, X.; Schneider, A.; et al. Effects of heat waves on mortality: Effect modification and confounding by air pollutants. *Epidemiology* **2014**, *25*, 15–22. [CrossRef] [PubMed]

15. Huang, H.; Deng, X.; Yang, H.; Li, S. Spatial evolution of the effects of urban heat island on residents' health. *Tehnički Vjesnik* **2020**, *27*, 1427–1435.
16. Orru, H.; Ebi, K.; Forsberg, B. The interplay of climate change and air pollution on health. *Curr. Environ. Health Rep.* **2017**, *4*, 504–513. [CrossRef] [PubMed]
17. Alcock, I.; White, M.; Cherrie, M.; Wheeler, B.; Taylor, J.; McInnes, R.; Im Kampe, E.O.; Vardoulakis, S.; Sarran, C.; Soyiri, I.; et al. Land cover and air pollution are associated with asthma hospitalisations: A cross-sectional study. *Environ. Int.* **2017**, *109*, 29–41. [CrossRef] [PubMed]
18. Calia, G.; Ledda, A.; Serra, V.; Senes, G.; De Montis, A. GI Guidelines for the Metropolitan City of Cagliari (Italy): A Method for Implementing Green Areas. *Appl. Sci.* **2021**, *11*, 10863. [CrossRef]
19. Beute, F.; Marselle, M.R.; Olszewska-Guizzo, A.; Andreucci, M.; Lammel, A.; Davies, Z.G.; Glanville, J.; Keune, H.; O'Brien, L.; Remmen, R.; et al. How do different types and characteristics of green space impact mental health? A scoping review. *People Nat.* **2023**, *5*, 1839–1876. [CrossRef]
20. Menconi, M.; Abbate, R.; Simone, L.; Grohmann, D. Urban Green System Planning Insights for a Spatialized Balance between PM10 Dust Retention Capacity of Trees and Urban Vehicular PM10 Emissions. *Sustainability* **2023**, *15*, 5888. [CrossRef]
21. Choudhury, M.A.M.; Marcheggiani, E.; Galli, A.; Modica, G.; Somers, B. Mapping the urban atmospheric carbon stock by lidar and worldview-3 data. *Forests* **2021**, *12*, 692. [CrossRef]
22. Castelo, S.; Amado, M.; Ferreira, F. Challenges and Opportunities in the Use of Nature-Based Solutions for Urban Adaptation. *Sustainability* **2023**, *15*, 7243. [CrossRef]
23. Dardir, M.; Wilson, J.; Berardi, U. Heat and air quality related cause-based elderly mortalities and emergency visits. *Environ. Res.* **2023**, *216*, 114640. [CrossRef]
24. Ulpiani, G. On the linkage between urban heat island and urban pollution island: Three-decade literature review towards a conceptual framework. *Sci. Total Environ.* **2021**, *751*, 141727. [CrossRef]
25. Taherdoost, H.; Madanchian, M. Multi-criteria decision making (MCDM) methods and concepts. *Encyclopedia* **2023**, *3*, 77–87. [CrossRef]
26. de Almeida, A.T.; Alencar, M.H.; Garcez, T.V.; Ferreira, R.J.P. A systematic literature review of multicriteria and multi-objective models applied in risk management. *IMA J. Manag. Math.* **2017**, *28*, 153–184. [CrossRef]
27. Lyu, H.M.; Yin, Z.Y. An improved MCDM combined with GIS for risk assessment of multi-hazards in Hong Kong. *Sustain. Cities Soc.* **2023**, *91*, 104427. [CrossRef]
28. Lyu, H.M.; Yin, Z.Y.; Zhou, A.; Shen, S.L. MCDM-based flood risk assessment of metro systems in smart city development: A review. *Environ. Impact Assess. Rev.* **2023**, *101*, 107154. [CrossRef]
29. Zheng, Q.; Shen, S.L.; Zhou, A.; Lyu, H.M. Inundation risk assessment based on G-DEMATEL-AHP and its application to Zhengzhou flooding disaster. *Sustain. Cities Soc.* **2022**, *86*, 104138. [CrossRef]
30. Sangiorgio, V.; Uva, G.; Fatiguso, F. Optimized AHP to overcome limits in weight calculation: Building performance application. *J. Constr. Eng. Manag.* **2018**, *144*, 04017101. [CrossRef]
31. Almeida, C.R.d.; Teodoro, A.C.; Gonçalves, A. Study of the urban heat island (UHI) using remote sensing data/techniques: A systematic review. *Environments* **2021**, *8*, 105. [CrossRef]
32. Li, Y.; Schubert, S.; Kropp, J.P.; Rybski, D. On the influence of density and morphology on the Urban Heat Island intensity. *Nat. Commun.* **2020**, *11*, 2647. [CrossRef]
33. Wu, H.; Huang, B.; Zheng, Z.; Sun, R.; Hu, D.; Zeng, Y. Urban anthropogenic heat index derived from satellite data. *Int. J. Appl. Earth Obs. Geoinf.* **2023**, *118*, 103261. [CrossRef]
34. Rao, P.; Singh, A.; Pandey, K. Time-series analysis of open data for studying urban heat island phenomenon: A geospatial approach. *Spat. Inf. Res.* **2021**, *29*, 907–918. [CrossRef]
35. Bell, S.L.; Phoenix, C.; Lovell, R.; Wheeler, B.W. Green space, health and wellbeing: Making space for individual agency. *Health Place* **2014**, *30*, 287–292. [CrossRef]
36. Kottek, M.; Grieser, J.; Beck, C.; Rudolf, B.; Rubel, F. World map of the Köppen-Geiger climate classification updated. *Meteorol. Z.* **2006**, *15*, 259–263. [CrossRef]
37. Nistor, M.M. Spatial distribution of climate indices in the Emilia-Romagna region. *Meteorol. Appl.* **2016**, *23*, 304–313. [CrossRef]
38. Amani, M.; Ghorbanian, A.; Ahmadi, S.A.; Kakooei, M.; Moghimi, A.; Mirmazloumi, S.M.; Moghaddam, S.H.A.; Mahdavi, S.; Ghahremanloo, M.; Parsian, S.; et al. Google earth engine cloud computing platform for remote sensing big data applications: A comprehensive review. *IEEE J. Sel. Top. Appl. Earth Obs. Remote. Sens.* **2020**, *13*, 5326–5350. [CrossRef]
39. Balan, R.; Rao, P.; Gupta, K.; Roy, A. Open Source Google Earth Platform for Computation of Heat Wave Indicators. Paper Presented at Free and Open Source Software for Geospatial (FOSS4G) 2020. 2020. Available online: https://www.researchgate.net/publication/353400581_Open_Source_Google_Earth_Platform_for_Computation_of_Heat_Wave_Indicators (accessed on 15 November 2023).
40. Rao, P.; Gupta, K.; Roy, A.; Balan, R. Spatio-temporal analysis of land surface temperature for identification of heat wave risk and vulnerability hotspots in Indo-Gangetic Plains of India. *Theor. Appl. Climatol.* **2021**, *146*, 567–582. [CrossRef]
41. Nieves, J.J.; Bondarenko, M.; Kerr, D.; Ves, N.; Yetman, G.; Sinha, P.; Clarke, D.J.; Sorichetta, A.; Stevens, F.R.; Gaughan, A.E.; et al. Measuring the contribution of built-settlement data to global population mapping. *Soc. Sci. Humanit. Open* **2021**, *3*, 100102. [CrossRef]

42. Bondarenko, M.; Kerr, D.; Sorichetta, A.; Tatem, A.; WorldPop. *Estimates of 2020 Total Number of People per Grid Square, Adjusted to Match the Corresponding UNPD 2020 Estimates and Broken down by Gender and Age Groupings, Produced Using Built-Settlement Growth Model (BSGM) Outputs*; University of Southampton: Southampton, UK, 2020.
43. Demuzere, M.; Kittner, J.; Martilli, A.; Mills, G.; Moede, C.; Stewart, I.D.; van Vliet, J.; Bechtel, B. A global map of Local Climate Zones to support earth system modelling and urban scale environmental science. *Earth Syst. Sci. Data Discuss.* **2022**, *2022*, 1–57. [CrossRef]
44. Fever, S.K.; Kahl, J.D.; Kalkbrenner, A.E.; Cerón Bretón, R.M.; Cerón Bretón, J.G. A New Combined Air Quality and Heat Index in Relation to Mortality in Monterrey, Mexico. *Int. J. Environ. Res. Public Health* **2022**, *19*, 3299. [CrossRef]
45. Xu, H.; Brook, R.D.; Wang, T.; Song, X.; Feng, B.; Yi, T.; Liu, S.; Wu, R.; Chen, J.; Zhang, Y.; et al. Short-term effects of ambient air pollution and outdoor temperature on biomarkers of myocardial damage, inflammation and oxidative stress in healthy adults. *Environ. Epidemiol.* **2019**, *3*, e078. [CrossRef]
46. Saaty, T.L. How to make a decision: The analytic hierarchy process. *Eur. J. Oper. Res.* **1990**, *48*, 9–26. [CrossRef]
47. WMO. *Global Warming of 1.5 °C*; World Meteorological Organization: Geneva, Switzerland, 2018.
48. Chen, B.; Xie, M.; Feng, Q.; Li, Z.; Chu, L.; Liu, Q. Heat risk of residents in different types of communities from urban heat-exposed areas. *Sci. Total Environ.* **2021**, *768*, 145052. [CrossRef]
49. Lopez-Bueno, J.A.; Díaz, J.; Sánchez-Guevara, C.; Sánchez-Martínez, G.; Franco, M.; Gullón, P.; Peiró, M.N.; Valero, I.; Linares, C. The impact of heat waves on daily mortality in districts in Madrid: The effect of sociodemographic factors. *Environ. Res.* **2020**, *190*, 109993. [CrossRef]
50. Fischer, P.H.; Brunekreef, B.; Lebret, E. Air pollution related deaths during the 2003 heat wave in the Netherlands. *Atmos. Environ.* **2004**, *38*, 1083–1085. [CrossRef]
51. Van Ryswyk, K.; Prince, N.; Ahmed, M.; Brisson, E.; Miller, J.D.; Villeneuve, P.J. Does urban vegetation reduce temperature and air pollution concentrations? Findings from an environmental monitoring study of the Central Experimental Farm in Ottawa, Canada. *Atmos. Environ.* **2019**, *218*, 116886. [CrossRef]
52. Jain, S.; Sannigrahi, S.; Sen, S.; Bhatt, S.; Chakraborti, S.; Rahmat, S. Urban heat island intensity and its mitigation strategies in the fast-growing urban area. *J. Urban Manag.* **2020**, *9*, 54–66. [CrossRef]
53. Melaas, E.K.; Wang, J.A.; Miller, D.L.; Friedl, M.A. Interactions between urban vegetation and surface urban heat islands: a case study in the Boston metropolitan region. *Environ. Res. Lett.* **2016**, *11*, 054020. [CrossRef]
54. Semenzato, P.; Bortolini, L. Urban Heat Island Mitigation and Urban Green Spaces: Testing a Model in the City of Padova (Italy). *Land* **2023**, *12*, 476. [CrossRef]
55. Zhang, Y.; Wang, Y.; Ding, N.; Yang, X. Assessing the Contributions of Urban Green Space Indices and Spatial Structure in Mitigating Urban Thermal Environment. *Remote. Sens.* **2023**, *15*, 2414. [CrossRef]
56. Huang, X.; Liu, J.; Zhu, W.; Atzberger, C.; Liu, Q. The optimal threshold and vegetation index time series for retrieving crop phenology based on a modified dynamic threshold method. *Remote. Sens.* **2019**, *11*, 2725. [CrossRef]